Effects of Drought on the Relationship Between Photosynthesis and Chlorophyll Fluorescence for Maize

Jidai Chen, Xinjie Liu, ShanShan Du, Yan Ma, and Liangyun Liu

***Abstract*—Structural–physiological factors affect the accurate estimation of vegetation gross primary production (GPP) under various types of environmental stress. Solar-induced chlorophyll fluorescence (SIF), which is directly linked to photosynthesis, has been effectively used to estimate and monitor GPP. However, understanding of the physiological mechanism linking SIF to GPP under stress remains limited. In this article, the link between SIF and GPP at diurnal and seasonal timescales was explored for a maize field and its response to drought stress (as defined by the crop water stress index, CWSI) using three-years of continuous tower-based measurements was investigated. The results show that the ratio of GPP to SIF decreased with increasing drought stress levels, and the canopy stomata conductance (Gs) declined synchronously. Compared to two canopy structural factors (NDVI and NIRv), both the Pearson and partial correlation coefficients for the relationship between Gs and the ratio of GPP to the total SIF was higher (0.38, $p < 0.01$ and 0.32, $p < 0.01$ with photosynthetically active radiation as the control variable, respectively). We also found that Φ_F tracked the changes in LUE well under drought conditions (CWSI > 0.6), which demonstrated that SIF can be a powerful parameter for estimating GPP under drought stress. However, there was a smaller drop in Φ_F under drought stress (slope $=$ –0.002) compared to the slope for the relationship between LUE and CWSI (–0.08). The response of light reactions to drought stress may be muted compared to the stomatal response. These findings confirm that the Gs is sensitive to drought and is important for the SIF-based GPP estimation model. It also provides reliable evidence that SIF data include a large amount of physiological information and can serve as a potential indicator for detecting drought and estimating GPP.**

***Index Terms*—Chlorophyll fluorescence, crop water stress index (CWSI), drought, gross primary production, maize.**

Manuscript received June 14, 2021; revised September 22, 2021 and October 23, 2021; accepted October 23, 2021. Date of publication October 27, 2021; date of current version November 12, 2021. This work was supported in part by the National Key Research and Development Program of China under Grant 2017YFA0603001 and in part by the National Natural Science Foundation of China under Grant 42071310 and Grant 41825002. *(Corresponding author: Xinjie Liu.)*

Jidai Chen is with the Aerospace Information Research Institute, Chinese Academy of Sciences, Beijing 100094, China, and also with the University of Chinese Academy of Sciences, Beijing 100049, China (e-mail: chenjidai@aircas.ac.cn).

Xinjie Liu, ShanShan Du, Yan Ma, and Liangyun Liu are with the University of Chinese Academy of Sciences, Beijing 100049, China (e-mail: liuxj@radi.ac.cn; duss@radi.ac.cn; mayan2017@radi.ac.cn; liuly@radi.ac.cn).

This article has supplementary downloadable material available at https://doi.org/10.1109/JSTARS.2021.3123111, provided by the authors.

Digital Object Identifier 10.1109/JSTARS.2021.3123111

I. Introduction

PHOTOSYNTHESIS is associated with one of the largest carbon dioxide fluxes and is the most important biochemical process in terrestrial ecosystems; thus, the measurement of photosynthetic carbon uptake plays an important role in understanding the global carbon cycle [1]–[5]. The response of gross primary productivity (GPP) to climate has been shown to vary across space and time. This effect has been hypothesized to be the result of the interaction between multiple bioclimatic factors, including environmental energy (i.e., temperature and radiation) and water availability. Drought stress is a significant issue that affects plant photosynthesis [6]. Conventional remote sensing techniques, such as optical, thermal infrared, and microwave remote sensing, have been extensively used to estimate soil moisture status by exploiting the surface reflection, surface temperature, and backscatter coefficient. However, uncertainties remain in estimates of instantaneous vegetation stresses because of a lack of information about plant physiological status.

Solar-induced chlorophyll fluorescence is directly related to vegetation photosynthesis and has been used as a powerful, nondestructive, and reliable tool in detecting vegetation physiological changes and the effects of environmental stress on photochemistry at different spatiotemporal scales [7], [8]. The photosynthetic active radiation absorbed by plant chlorophyll (APAR) has several dissipation pathways, with the largest of these involving photochemical processes [9]. However, excess absorbed light is also released in a variety of nonphotochemical quenching (NPQ) processes and triggers the chlorophyll to emit fluorescence at longer wavelengths (650–800 nm). These de-excitation processes are mutually exclusive and their relative proportions can be expressed, as shown in [10]

$$1 = \Phi_P + \Phi_{\mathrm{NPQ}} + \Phi_F + \Phi_D \tag{1}$$

here, Φ_P is the proportion of the energy used in photochemical processes, Φ_{NPQ} is the proportion of energy dissipated by NPQ, Φ_F is the proportion of energy dissipated as fluorescence, and Φ_D is the basic heat dissipation. The intensity of the fluorescence light emitted primarily by chlorophyll-a in the antennae system of photosystem 2 (PSII) depends on the number of excited electrons in the light reactions and is, therefore, related to the functional status of the PSII and NPQ. Therefore, the physiological link between SIF and GPP under stress is already a topic of research.

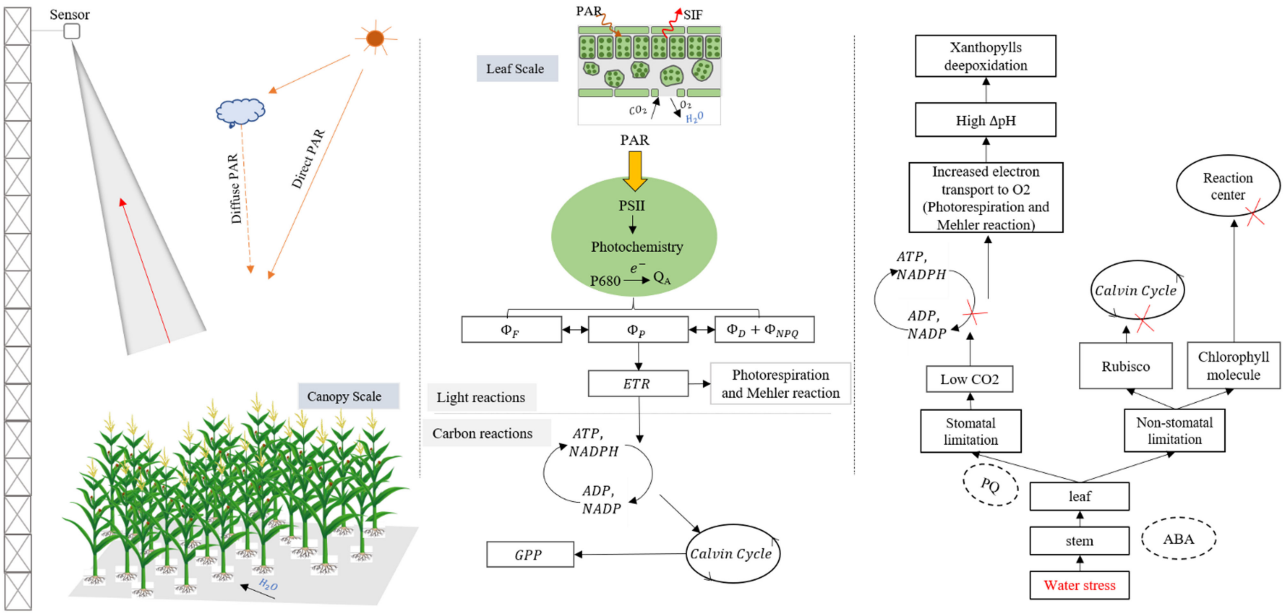

Fig. 1. Simple overview of the link between photosynthesis and chlorophyll fluorescence at the leaf and canopy level and its response to water stress in the soil–plant–atmosphere continuum. To some extent, this explains the observed interrelationships between different photosynthetic processes. (The X indicates a negative effect – see text for more details. The dotted ellipse represents the elements affected by drought stress).

However, there is considerable uncertainty in the SIF–GPP relationship under environmental stress (mainly related to light, temperature, and water availability) at different spatiotemporal scales and for different species. Accurate quantification of GPP and its spatial–temporal distribution under changing environmental conditions and at different scales (from the canopy to the global scale) remains a challenge [11]. Among these environmental factors, water availability is a key factor that affects the down-regulation of plant productivity. Because the light and carbon reactions in photosynthesis might decouple at different timescales under environmental stress [12], the relationship between SIF and GPP under drought stress is still complex and is the subject of some disagreement [13], [14].

One of the uncertainties affecting the SIF-GPP relationship relates to the stomatal response to drought—this may be faster than the electron transfer response and so may change the SIF–GPP relationship [12]. Under drought conditions, the rapid closure of stomata result in less CO_2 entering the chloroplasts and a drop in the CO_2/O_2 ratio, thereby increasing the rate of photorespiration and/or the Mehler reaction. Since these processes consume relatively less ATP than does photosynthesis, this should lead to a definite increase of trans-thylakoid ΔpH [15], [16]. The xanthophyll de-epoxidation that follows an increase in ΔpH should then lead to an increase in NPQ. Thus, thermal dissipation in the antennae becomes progressively more important and fluorescent emission is consequently lowered (see Fig. 1). Souza *et al.* [17] demonstrated that, as a result of water stress, cowpea can avoid tissue dehydration by closing stomata to maintain a high leaf-water potential or a high leaf relative water content. There was a fall in the value of the photosynthetic parameters as a result of the drought stress and both stomatal and nonstomatal reactions limited the photosynthesis. It was also discovered that the down-regulation of photosynthesis under medium water stress might be attributable to stomatal limit and that the nonstomatal limitations might be the main factor leading to decreased photosynthesis. This is because severe water stress can seriously affect the activity and activation state of Rubisco and chloroplasts [18]. Helm *et al.* [19] also reported that the reduced CO_2 assimilation in response to drought may be attributable to the closure of stomata restricting the amount of CO_2 entering the leaves (stomatal restriction) or causing leaf biochemical changes to inhibit or down-regulate photosynthesis (nonstomatal restriction); there was observed to be smaller decrease in fluorescence than in the amount of CO_2 assimilation. The incongruity of light and carbon reactions is one reason for the complex relationship between GPP and SIF as SIF is directly related to light reactions other than those that are part of the carbon process.

The other main factor affecting the SIF–GPP relationship concerns the complex regulation mechanism between Φ_P, Φ_{NPQ} and Φ_F in the light reactions under drought stress (see Fig. 1). Any biotic and abiotic stress can affect the function of PSII, which in turn affects the SIF. A large number of studies have demonstrated that biotic and abiotic stressors affect the photosynthetic performance of leaves and modify their optical and fluorescent properties at leaf levels [e.g., 18]. The limits on photosynthesis that result from stomatal closure along with an increase in NPQ and photorespiration (PR) change the balance between PSII and the electron demand, resulting in overexcitation and subsequent photo-inhibitory damage in light reactions [20]. In this way, SIF and GPP might respond differently to drought conditions, since SIF is more closely related to PSII reactions centers. Based on an assessment of chlorophyll-a fluorescence in cowpea, Souza *et al.* [17] found that PSII is quite resistant to water deficits based on assessment chlorophyll a fluorescence in cowpea. In addition, earlier studies have demonstrated

that the morphological and physiological responses to drought vary considerably among species [21], and that the effects of drought stress on fluorescence are especially pronounced in maize since, as a C4-type plant that has a different metabolism from C3-type plants, the PR is much weaker [22]. In addition, some of these fluorescent parameters have proven to be related to Gs determined at a given light intensity [23], [24]. Busch [25] recently proposed that instead of a photosynthesis-derived signal, the redox state of the chloroplast plastoquinone pool might be signaled to the stomatal guard cells. Consistent with this hypothesis, Kromdijk *et al.* [26] also observed tightly and linearly coordinated changes in the redox state of quinone A (Q_A), as estimated from the fluorescence parameter (q_L) and stomatal conductance (Gs) in tobacco with modified levels of photosystem II subunit S, which has been shown to be a strong determinant of the amplitude of nonphotochemical quenching and, therefore, also affects the redox state of the chloroplast electron transport chain (see Fig. 1). Therefore, Gs might be a sensitive indicator for the responses of GPP and SIF to drought stress; thus, in the estimation of GPP, the effects of drought on reductions in the uncertainties in the SIF-based models should be considered.

Additionally, SIF-based GPP models are significantly affected by interactions of the canopy structure and plant physiological changes. GPP is generally expressed as a semiempirical light-use efficiency framework [27], where APAR and the light-use efficiency (denoted as LUE: $\mathrm{GPP} = \mathrm{APAR} \times \mathrm{LUE}$) represent structural and physiological information, respectively [28]. Similarly, SIF can be expressed as the product of APAR and the fluorescence quantum yield (SIF yield, $\mathrm{SIF} = \mathrm{APAR} \times \mathrm{SIF}_{\mathrm{yield}}$). Previous studies have found that the close relationship between SIF and GPP is largely attributable to APAR, whereas the key issue for GPP estimation based on SIF measurements is the link between LUE and $\mathrm{SIF}_{\mathrm{yield}}$, which remains unclear under changeable environmental conditions [29]–[32]. Furthermore, some researchers have reported that the near-infrared (NIR) radiance of vegetation (NIRvRad, the product of the reflectance in the near-infrared band, the normalized difference vegetation index (NDVI), and the incident radiance) can be used to produce good estimates of the GPP as it contains a large amount of information about the canopy structure [33], [34]. However, information about the physiological response to short-lived environmental stress is still lacking. Therefore, SIF, which can be used as a probe for studying photosynthesis and which reacts rapidly to changeable environmental conditions, can be an effective tool for accurately estimating GPP at the global scale.

Long-term tower-based measurements provide us an opportunity for better understanding the link between canopy SIF and GPP, especially under varying environmental conditions. During the last decade, various indexes have been developed to monitor water stress in plants [35]. The crop water deficit index (CWSI), developed using the temperature difference between the air and canopy have been successfully used for drought detection. Infrared thermometers are commonly used to measure the canopy temperature. The maximum amount of plant transpiration occurs when there is sufficient moisture in the root zone. The transpiration cools the leaves and the leaf temperature will be lower than the ambient temperature. As a result of drought stress, plants close stomata and the energy dissipation is interrupted; this results in a rise in leaf temperature such that it exceeds the ambient temperature [36]. Although the CWSI does not consider the effects of sunlit and shaded leaves, which may result in some uncertainty in drought detection, it has been shown to be an effective indicator of drought in crops [37].

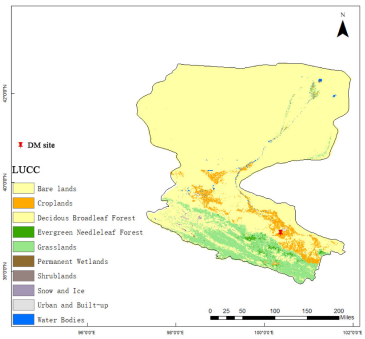

Fig. 2. Land use and cover classification for the Heihe River Basin; the red symbol represents the observation superstation (DM).

In this article, the effects of drought on photosynthesis and SIF were analyzed using measurements that covered the whole of the growing periods of 2017, 2018, and 2019 for a maize field. The drought stress was defined using the CWSI. The main objects of the article were to answer the following questions.

1) What are the details of the differences in the response of the SIF and GPP to drought at diurnal and seasonal timescales?
2) How does the GPP–SIF relationship change under drought stress?
3) What is the influence of the ecosystem conductance on the GPP–SIF relationship under drought stress?

II. Materials and Methods

A. Filed Measurements

1) Experimental Site: The study area was located within the Da Man site (DM) site at 100.372 °E, 38.856 °N in the middle reaches of the Heihe River Basin, approximately 8 km to the southeast of the Zhangye City, Gansu Province, China (see Fig. 2). The study area consisted of a typical irrigated maize crop. The DM site is equipped with a comprehensive observation system, including flux, meteorological, hydrological, and spectral instruments [38].

The DM site has a typical temperate continental climate with sparse and concentrated precipitation. The average annual temperature is 8 °C, the total sunshine duration is 3000–3600 h and the total annual precipitation is about 300 mm. The main crop type is monocropping maize, which is grown without specialized irrigation or fertilization controls. The soil type is sandy according to the HWSD map and using the FAO 90 classification system [39]. In terms of the soil particle composition, in the surface (0–5 cm) soil layer, the clay content is 21%, the sand content is 29% and the silt fraction is 50% (Fig. S1).

2) Measurements of Fluxes and Meteorological Parameters: The carbon dioxide (CO_2) exchange between the maize canopy and the atmosphere was measured using the eddy covariance (EC) technique. A high-frequency open-path infrared gas analyzer (IRGA) was placed on a 5-m high platform along with a three-dimensional sonic anemometer used to measure high-frequency instantaneous wind velocity components and the sonic temperature. The turbulence data were sampled at a frequency of 10 Hz and stored by a data logger (YK and GT CR5000, Campbell Scientific Corporation, Logan, Utah, USA). Detailed processing was then carried out on all the collected data: this included conversions, corrections, and plausibility tests.

The IRGA was also used to measure water vapor (LI-7500, LICOR Biosciences Inc., Lincoln, NE, USA). The turbulent fluxes of latent heat (LE) and sensible heat (H) were then computed as the covariance between the instantaneous vertical wind velocity, sonic temperature, and water vapor density. In addition, the LE and H fluxes was corrected by using the temperature (Ta) and air density in the coordinate rotating method, which is based on the Webb–Pearman–Leuning algorithm [40]. The measured ET is an important parameter used to characterize the water demand status of plants and is an indicator of drought.

Soil moisture is another key variable in the terrestrial system and exhibits complex changes over spatiotemporal scales. Accurate soil moisture values are essential to the management of irrigated crops and the assessment of drought stress. The soil volume moisture content (SWC), the area average of soil moisture at the hectometer horizontal scale, was measured using the newly developed cosmic ray probe (CRP), which was 0.5 m away from the ground and sampling data per hour. A negative correlation between near-surface fast neutron counts (produced by secondary cosmic-ray particles, in the soil) and soil moisture contents enables the use of the CRP to sense soil moisture. The CRP has a radius of about 300 m horizontal footprint. This instrument is located at the Heihe Watershed Allied Telemetry Experimental Research (HiWATER), which lies within the irrigated cropland area at the Zhangye Oasis. Some studies have reported that the real soil moisture at the field scale could be better estimated using the CRP rather than traditional point observations that use electromagnetic soil moisture sensors, hydro-geophysical methods, and active and passive microwave remote sensing [41], [42]. However, in this article, many SWC measurements in the peak growth periods were missing due to instrument breakdowns (see Fig. S5b).

The meteorological parameters were measured by an automatic weather station (AWS), also mounted on the EC flux tower. The AWS consisted of a meteorological gradient observation system that made continuous measurements of the photosynthetically active radiation (PAR), air temperature (T_a), humidity, precipitation, air pressure, the four radiation components (used for calculating the fraction of the radiation absorbed by plant chlorophyll), the soil heat flux, etc.

3) Measurements of Canopy Spectra: An automatic long-term observation system—an Ocean Optics QE65pro spectrometer (Ocean Optics, Dunedin, FL, USA)—that had a spectral resolution of ∼0.34 nm between 645 and 805 nm was fixed to a 25-m high platform. The Ocean Optics QE65pro spectrometer has a high a sampling interval of about 0.17 nm and a signal-to-noise ratio greater than 1000, which allows for better extraction of the fluorescence information. A cosine corrector (CC3-3-UV-S; Ocean Optics, Inc., Dunedin, FL, USA) and a conical fore-optic (bare fiber) were used to capture the downwelling incident radiance and upwelling radiance, respectively. The former has a large field view (FOV) of 180° and the latter can make measurements within a small FOV of about 25°. To reduce the influence of rapidly changing light conditions, we set the measurement mode to a "sandwich" type: i.e., by alternating the up and down channels, the spectrometer first measured the solar irradiance, then the radiance reflected by the canopy and finally the solar irradiance again. Before each measurement cycle, the integration time was optimized depending on the light conditions. Generally, a complete spectral observation took about 15 s at midday and about 2 min at sunrise or sunset.

The spectral measurements at the DM site were conducted from June 7, 2017 to September 30, 2017; June 1, 2018 to September 29, 2018; and June 2, 2019 to September 30, 2019. For 2017, some data were missing (for the periods July 12 to 22 and August 22 to September 10) due to hardware failure. Similarly, data were not collected from June 11 to June 18 in 2019. In total, we obtained 308 days of valid data at the DM site during the growing seasons of 2017, 2018, and 2019.

B. Data Processing

1) Calculation of GPP and LUE: The flux GPP was extracted from the difference between the ecosystem respiration (Re) and the EC-measured net ecosystem exchange of CO_2 (NEE) using the method generally referred to as the daytime flux partitioning algorithm proposed by Reichstein *et al.* [43] (2). We used an online calculation tool[1] provided by the Max Planck Institute for Biogeochemistry, Germany to implement this algorithm [44] then obtained the half-hourly GPP data by data elimination, interpolation, and partition. Finally, we used a simple averaging method to obtain the daily mean data [45]. In this article, we used the $\mathrm{GPP_{flux}}$ data as the true GPP values

$$\mathrm{GPP_{flux}} = \mathrm{NEE} - \mathrm{Re}. \tag{2}$$

The photosynthetically active radiation (PAR) was continuously measured by an AWS, also mounted on the EC flux tower. The $f\mathrm{PAR}$ data, the fraction of APAR, were collected using an $f\mathrm{PAR_{net}}$ system [46]. Observations of four components of PAR were observed using $f\mathrm{PAR_{net}}$: these components consisted of the total downward PAR arriving at the top of the maize canopy ($\mathrm{PAR}_{\downarrow \mathrm{ac}}$), the PAR reflected by the canopy ($\mathrm{PAR}_{\uparrow \mathrm{ac}}$), the PAR transmitted to the soil background ($\mathrm{PAR}_{\downarrow \mathrm{BC}}$) and the PAR reflected by soil ($\mathrm{PAR}_{\uparrow \mathrm{BC}}$). The observed PAR values measured by nine independent sensors were averaged to reduce noise. Thus, the canopy fPAR could be calculated using the four PAR components [46]

$$f\mathrm{PAR_{net}} = \frac{(\mathrm{PAR}_{\uparrow \mathrm{ac}} - \mathrm{PAR}_{\downarrow \mathrm{ac}}) - (\mathrm{PAR}_{\uparrow \mathrm{BC}} - \mathrm{PAR}_{\downarrow \mathrm{BC}})}{\mathrm{PAR}_{\uparrow \mathrm{ac}}}. \tag{3}$$

[1][Online]. Available: https://www.bgc-jena.mpg.debgiindex.php/Services/REddyProcWeb

However, due to the large number of missing $f\mathrm{PAR}$ measurements, we used a model based on the normalized difference vegetation index (NDVI) to estimate $f\mathrm{PAR}$. Previous studies have found that the $f\mathrm{PAR}$–NDVI relationship appears to be unaffected by the solar elevation angle (θ_s) for a fixed viewing angle [46]–[49]. We then obtained fPAR values from the continuous NDVI data calculated from the spectrum data (5) as follows:

$$\mathrm{NDVI} = \frac{\rho_{nir} - \rho_{\mathrm{red}}}{\rho_{nir} - \rho_{\mathrm{red}}} \tag{4}$$

$$f\mathrm{PAR}_{\mathrm{NDVI}} = \frac{(\mathrm{NDVI} - \mathrm{NDVI}_{\min})\,(f\mathrm{PAR}_{\max} - f\mathrm{PAR}_{\min})}{\mathrm{NDVI}_{\max} - \mathrm{NDVI}_{\min}} + f\mathrm{PAR}_{\min} \tag{5}$$

here, ρ_{nir} is the near-infrared reflectance (800 nm) and ρ_{red} is the reflectance at the red band (680 nm). For the maize crop in our study area, $\mathrm{NDVI}_{\max} = 0.95$, $\mathrm{NDVI}_{\min} = 0.22$, $f\mathrm{PAR}_{\max} = 0.95$, and $f\mathrm{PAR}_{\min} = 0.05$.

To evaluate the performance of the NDVI-based $f\mathrm{PAR}$ model, we used the $\mathrm{fPAR}_{\mathrm{net}}$ data as a validation dataset. The validated results also showed that the NDVI can be used to estimate changes in fPAR ($R^2 = 0.77$, RMSE $= 0.08$; Fig. S2). Using a semiempirical framework, we then calculated the LUE as

$$\mathrm{LUE} = \frac{\mathrm{GPP}}{\mathrm{PAR} \times f\mathrm{PAR}}. \tag{6}$$

2) Calculation of Canopy SIF and Φ_F: The Canopy SIF ($\mathrm{SIF}_{\mathrm{canopy}}$) at the O2-A band (centered at 760 nm) was calculated using the differential optical absorption spectroscopy (DOAS) algorithms and was averaged over 30-min intervals between sunrise and sunset [45], [50]. DOAS has been demonstrated to be a reliable method for ground-based SIF retrieval [51]. DOAS models use a combination of polynomials and the fluorescence spectrum (h_F) shape normalized by the reflected irradiance. In this article, the DOAS algorithm was configured to model the logarithm of the apparent reflectance in the Fraunhofer fitting window (745–759 nm) using sixth-order order Legendre polynomials and an assumed h_F. The DOAS algorithm can be expressed as [7], [51]–[53]

$$D = \log\left(\frac{L}{E}\right) \approx \sum_{n=0}^{6} P_n\left(\frac{\lambda}{\max(|\lambda|)}\right) + \frac{h_F}{L} \tag{7}$$

where D represents the optical density, L is the irradiance upwelling from the surface, E is the incoming solar irradiance, and P_n is the Legendre polynomial, h_F is the SIF emission spectrum, and λ is the retrieved band (here, 760 nm). Since the oxygen absorption lines are apparently influenced by the atmosphere, we used a look-up-table method to correct for the atmospheric effects [54]. Similarly, we averaged the canopy SIF to half-hourly values to correspond to the flux measurements. The canopy SIF is only part of the total SIF ($\mathrm{SIF}_{\mathrm{total}}$) emitted inside the leaves due to reabsorption and scattering within the canopy [30]. Thus, the retrieved canopy SIF needs to be downscaled to photosystem level so that it can better explain the SIF–GPP relationship. $\mathrm{SIF}_{\mathrm{total}}$ can be calculated as the ratio of $\mathrm{SIF}_{\mathrm{canopy}}$ to f_{esc} (the canopy SIF escape probability) [31], [55]

$$\mathrm{SIF}_{\mathrm{total}} = \frac{\mathrm{SIF}_{\mathrm{canopy}}}{f_{\mathrm{esc}}} \tag{8}$$

$$f_{\mathrm{esc}} \approx \frac{\mathrm{NIR}v}{f\mathrm{PAR}}. \tag{9}$$

Like the GPP, the SIF can also be expressed as the product of APAR and the "apparent" SIF yield. The apparent SIF yield consists of a structural parameter (f_{esc}) and a parameter containing physiological information (Φ_F). Φ_F is related to plant physiological mechanisms only and indicates the physiological responses to drought other than those involving canopy structural characteristics (the leaf area index, leaf inclination angle distribution, etc.). Φ_F can be calculated as follows [31], [32], [55]:

$$\mathrm{SIF}_{\mathrm{canopy}} = \mathrm{PAR} \times f\mathrm{PAR} \times \Phi_F \times f_{\mathrm{esc}} \tag{10}$$

$$\Phi_F \approx \frac{\mathrm{SIF}_{\mathrm{canopy}}}{\mathrm{PAR} \times \mathrm{NIR}v}. \tag{11}$$

3) Calculation of Canopy Conductance: The stomatal conductance (g_s) is the degree of stomatal opening at leaf level, which is the main factor affecting plant photosynthesis, respiration, and transpiration. The canopy conductance (G_s), an overall indicator of stomata in plant ecosystem, is the result of the leaf Gs being pushed up to the canopy scale. G_s was calculated by inverting the Penman–Monteith (PM) equation [27], [56] using the eddy-covariance data

$$G_s = \frac{\gamma g_a LE}{\Delta\,(R_n - G) + \rho c_p g_a \mathrm{VPD}_a - (\Delta + \gamma)\,LE} \tag{12}$$

where γ is the psychrometric constant ($Pa\ K^{-1}$), which is related to the pressure, g_a is the aerodynamic conductance ($m\ s^{-1}$), Δ is the slope of the saturation vapor pressure curve ($kPa\ K^{-1}$), LE is the latent heat flux ($W\ m^{-2}$), R_n is the net radiation ($W\ m^{-2}$), and G is the soil heat flux below the canopy ($W\ m^{-2}$). In addition, ρ is the density of air ($kg\ m^{-3}$), which depends on the temperature, pressure and humidity, c_p is the specific heat capacity of air ($kJ\ kg^{-1}\ K^{-1}$) and VPD_a is the atmospheric vapor pressure deficit, which is defined as the difference between the atmospheric vapor pressure at ambient temperature and the actual vapor pressure [57]. In this equation, the units of G_s are $m\ s^{-1}$ but these were transformed to $mol\ m^{-2}\ s^{-1}$ using the ideal gas law [58].

The g_a can be calculated from

$$g_a = \frac{k^2 * u}{\left[\ln\left(\frac{z-d+z_H}{z_H}\right) + \psi_H\right] * \left[\ln\left(\frac{z-d+z_M}{z_M}\right) + \psi_M\right]} \tag{13}$$

where z is the anemometer height (m), d is the zero-plane displacement (m), z_H and z_M indicate the roughness lengths for the sensible heat and momentum (m), respectively, and ψ_H and ψ_M represent the stability correction factors for the heat and momentum, respectively; k is the von Karman constant (0.41) and u is the wind speed at height z. Both d and z_M can be estimated as functions of the canopy height, h (2.5 m for maize at full canopy) and z_H as a function of z_M (generally $d =$

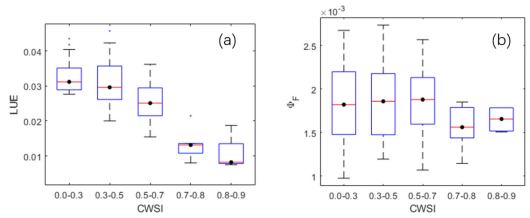

Fig. 3. Relationships between LUE (a), Φ_F (b) and CWSI in several intervals of CWIS.

0.67 h, $z_M = 0.67$ h, $z_H = 0.2z_M$). The stomata conductance (Gs) critically determines the photosynthetic uptake of CO_2 and the loss of water transpired from leaves.

4) Calculation of the Drought Index: We estimated the occurrence of drought using an effective indicator named the CWSI, which has been demonstrated to be effective for detecting drought in crops. In this article, we used the empirical method for calculation of the drought index. The empirical approach for calculating the CWSI uses two baseline temperature—the well-watered and nontranspiring canopy temperatures [59]. In our study, the canopy temperature was measured using an infrared thermometer that had a spectral range of 8–14 μm and a field of view of 4° [42]. The air temperature was also recorded at the same time as the canopy temperature measurements. The CWSI was then computed as

$$\mathrm{CWSI} = \frac{(T_c - T_a) - \Delta T_{\min}}{\Delta T_{\max} - \Delta T_{\min}} \tag{14}$$

where T_c is the plant canopy temperature, T_a is the air temperature, $\Delta T_{\min}$ is the minimum temperature difference which can be obtained from the nonwater-stressed baselines and $\Delta T_{\max}$ is the maximum temperature difference due to stomatal closure when the soil is dry (referred to as the lower baseline, which is considered to have a constant value of 5). The minimum temperature difference for a nonstressed canopy at a potential transpiring rate can be given as [60]

$$\Delta T_{\min} = \frac{(R_n - G)}{g_a \rho C_p} \frac{\gamma}{\Delta + \gamma} - \frac{\mathrm{VPD}_a}{\Delta + \gamma}. \tag{15}$$

The lower baseline of the CWSI can also be determined from a function of the vapor pressure deficit (VPD, Fig. S3). In addition, the CWSI can be expressed in terms of the evapotranspiration (ET) using a theoretical approach based on the energy balance model [36, see more information in the Supplemental Material]. Due to the large uncertainties in assessing the potential crop ET_p, we used an empirical approach to calculate the CWSI. We found that the ratio of the flux tower daily GPP to the GPP modeled using the maximum LUE (0.06 $mol\ CO_2\ mol^{-1}$ photon for unstressed conditions; Fig. S4) was correlated with the CWSI [33], [61]. The obviously negative relationship between $\frac{\mathrm{GPP_{flux}}}{\mathrm{GPP_{LUE}}}$ and the CWSI confirmed that this drought index can indicate the occurrence of drought.

In addition, we judged the different drought degrees based on the change curve of daily LUE and Φ_F to CWSI (see Fig. 3). CWSI less than 0.3 indicates not drought, greater than 0.3. CWSI greater than 0.3 and less than 0.6 is a slight drought. CWSI greater than 0.6 is a serious drought.

5) Quality Control: Quality control procedures were applied to the raw data before analyzing the effect of drought stress on the SIF–GPP relationship. Measurements outside the range of $\mu \pm 3\sigma$ (where μ and σ are the mean and standard deviation, respectively) were also excluded from the data processing, and the raw SIF values that were negative or higher than 2 mW/m^2/nm/sr were excluded. Also, where the solar zenith angle was greater than 80°, the data were not used in the subsequent analysis. Sunny and cloudy days were defined by the clearness index (CI) proposed by Chen *et al.* [62] (for more detailed information, see Appendix B). In addition, days with NDVI < 0.70 were excluded from the analysis to reduce the uncertainties of the CWSI calculation. It is difficult to separate canopy temperature into plant and soil early and late growth periods of plants.

C. Theoretical Basis

The SIF–GPP relationship can be expressed as a linear function based on the assumption that $\frac{\mathrm{LUE}}{\Phi_F}$ is a constant. However, the value of $\frac{\mathrm{LUE}}{\Phi_F}$ is strongly influenced by environmental factors. Based on the mechanistic link between the actual electron transport rate and the GPP and SIF, the relationships between the GPP and SIF can be interpreted using the mechanistic light response model proposed by Gu *et al.* [12]. In this article, we used maize, a typical C4 crop, as the research object. C4 species have proven to use pump mechanisms to concentrate CO_2 in the vicinity of Rubisco in the bundle sheath cells. Thus, for C4 plants, the LUE and Φ_F can be expressed as Gu *et al.* [12]

$$\mathrm{LUE} \approx \frac{1-x}{3} \times \frac{q_L \Phi_{\mathrm{PSII}_{\max}} \beta}{(1+\mathrm{NPQ})(1-\Phi_{\mathrm{PSII}_{\max}}) + q_L \Phi_{\mathrm{PSII}_{\max}}} \tag{16}$$

$$\Phi_F = \frac{(1-\Phi_{\mathrm{PSII}_{\max}})\beta}{(1+k_{DF})[(1+\mathrm{NPQ})(1-\Phi_{\mathrm{PSII}_{\max}}) + q_L \Phi_{\mathrm{PSII}_{\max}}]} \tag{17}$$

where x is the fraction of the total electron transport allocated to the mesophyll cells (often taken as 0.4), q_L is the fraction of open PSII reaction centers, Φ_{PSIImax} is the maximum photochemical quantum yield of PSII, k_{DF} represents the ratio k_D/k_F (the ratio of the first-order rate constant for fluorescence to that for constitutive heat, generally assumed to have a value of 19), and β is the fraction of the absorbed PAR allocated to PSII, which is assumed to have a value of 0.5 [12].

If we combine (16) and (17), $\frac{\mathrm{LUE}}{\Phi_F}$ can be calculated as

$$\frac{\mathrm{LUE}}{\Phi_F} \approx \frac{1-x}{3} \times q_L \times \frac{\Phi_{\mathrm{PSIImax}}}{1-\Phi_{\mathrm{PSIImax}}} (1+k_{DF}). \tag{18}$$

The value of Φ_{PSIImax} appears to be conserved under unstressed conditions but can change following extended (many hours to several days) exposure to stress. By contrast, changes in the environmental conditions produce instantaneous responses in q_L. Thus, q_L is important for understanding the dynamics of SIF and its relationships with photosynthesis under environmental stress; however, there have been very few studies of the effects of environmental conditions on q_L.

Based on the hypothesis that the redox state of the chloroplast plastoquinone A (Q_A, which can be estimated from the fluorescence parameter, q_L) might be signaled to the stomatal guard cells instead of a photosynthesis-derived signal [25], [26] and that q_L has the dominant effect on changes in the SIF–GPP relationship under environmental stress, the g_s might reflect the dynamics of the $\frac{\text{LUE}}{\Phi_F}$ ratio under drought stress. Thus, we assumed that there was a certain relationship between $\frac{\text{LUE}}{\Phi_F}$ and g_s under drought stress when light was stable (see the derivation formula in Appendix C), which could be expressed as

$$\frac{\text{LUE}}{\Phi_F} \propto g_s. \tag{19}$$

It should be noted that the $\frac{\text{LUE}}{\Phi_F}$ is proportional to g_s under constant PAR levels with the drought becoming severe. In this article, we focused on the canopy-level Gs and its ability to track the relationship between SIF and GPP under drought stress. Gs controls the transport of CO_2 from the atmosphere to plant leaves, where it is used in photosynthesis. It must be emphasized that a high degree of coregulation between Gs and photosynthesis is usually found [63]. Since Gs is responsive to all the external (soil water availability and VPD) and internal (ABA, xylem conductivity, leaf water status) factors related to drought, it represents a more integrated basis for determining the overall effects of drought than leaf water potential and relative water content. Gs is strongly affected by drought stress, which results in a down-regulation of the whole photosynthesis process caused by the decreased CO_2 availability [64]. As stomatal movements are generally regulated in a complex way by multiple factors and because of the uncertainties in the retrieval method, we took the daily mean canopy conductance as being a reprehensive value of Gs. Thus, in searching for a common pattern of photosynthetic response to drought, we used the daily mean Gs as an integrated parameter that reflected the drought stress experienced by plants [61], [65]–[67].

III. Results

A. Analysis of the Canopy Time-Series Measurements

1) Diurnal Response of SIF and GPP to Drought Stress: To avoid any influences due to differences in growth stage and rapid changes in weather conditions, we analyzed the diurnal changes in SIF and GPP under clear-sky conditions (no significant difference in PAR level; $p < 0.05$) under a slight drought ($0.3<\text{CWSI}<0.6$) and nondrought conditions on DOY 224 and 228 in 2017; these days had CWSI values of 0.43 and 0.05 (significance difference; $p < 0.01$), respectively. It was observed that fluctuations in the diurnal GPP and SIF were mainly driven by changes in PAR, whereas the diurnal SIF–GPP relationship varied between slight drought and drought days (see Fig. 4).

We observed that the GPP decreased at the same SIF level or the SIF increased at the same GPP level on drought days; this effect could also be demonstrated from the SCOPE simulation results (see Fig. S5a). It can be seen from Fig. 4 that the illumination of DOY228 after 11 A.M. is obviously weakened and unstable. Under slight drought conditions, Φ_F original from light reactions might be muted compared the carbon reaction

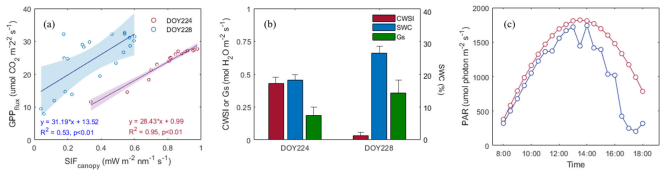

Fig. 4. (a) Relationship between SIF_{canopy} and GPP_{flux} for a drought day (red line; DOY 224) and nondrought day (blue line; DOY 228) based on measurements made in 2017. (b) Bar graph of CWSI, SWC, and Gs. (c) Diurnal changes of PAR. The shaded regions represent the 95% confidence levels for prediction.

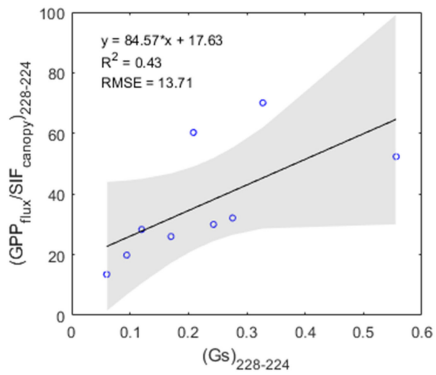

Fig. 5. Relationship between $(\frac{\text{GPP}_{\text{flux}}}{\text{SIF}_{\text{canopy}}})_{228-224}$ and $(\text{Gs})_{228-224}$. The black solid line represents the best fitted linear result. The shade area indicates the confidence region of 95%.

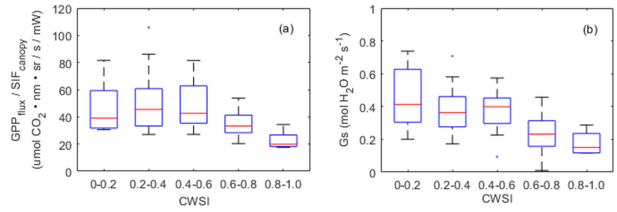

Fig. 6. (a) Boxplots showing (a) the ratio of $\text{GPP}_{\text{flux}}/\text{SIF}_{\text{canopy}}$ (equal to $\frac{\text{LUE}}{\Phi_F f_{\text{esc}}}$, (a) and (b) Gs, both plotted against with CWSI averaged over intervals of 0.2 for sunny days. Daily data with NDVI < 0.7 were excluded from the analysis.

(see Fig. 10). Therefore, the unstable light conditions might be the main reason for diurnal changes of SIF. In addition, the spectra were measured by altering the up and down channels and the integration time was automatically adjusted according to weather conditions. The temporal mismatch between the irradiance and radiance might also be a reason for daily maximum SIF of DOY224 higher than that of DOY228. The low value of G_s causing less CO_2 to be transported into the leaves resulted in the down-regulation of the carbon reaction process (see Fig. 4). Both the morning and afternoon data showed the same regular pattern (see Fig. S6).

In addition, we analyzed the instantaneous relationship between $(\frac{\text{GPP}_{\text{flux}}}{\text{SIF}_{\text{canopy}}})_{228-224}$ and $(\text{Gs})_{228-224}$ based on the (19) (see Fig. 5). The subscripts represent the difference of DOY228 and DOY224. After quality control, we can see the $(\frac{\text{GPP}_{\text{flux}}}{\text{SIF}_{\text{canopy}}})_{228-224}$ exhibited a good relationship with $(\text{Gs})_{228-224}$.

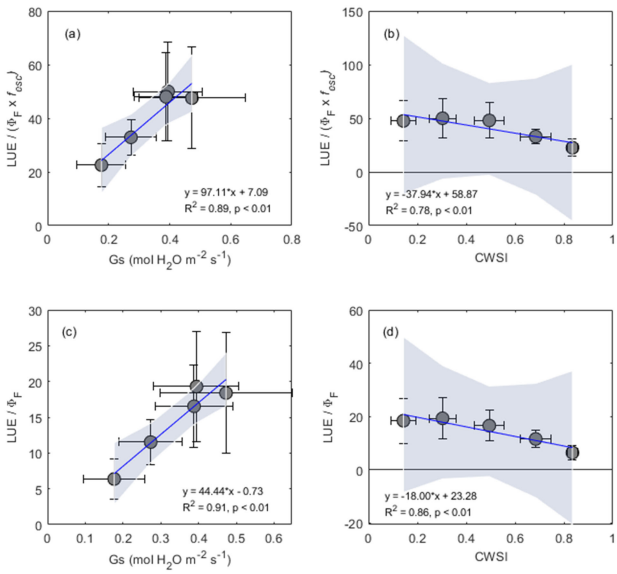

Fig. 7. Dependence of $\mathrm{LUE}/(\Phi_F \times f_{\mathrm{esc}})$ on (a) Gs and (b) CWSI averaged over intervals of 0.2 for sunny days; the correlation between LUE/Φ_F to (c) Gs and (d) CWSI. The blue lines represent the lines of best fit. Daily data with NDVI < 0.7 were excluded from the analysis. The shaded regions represent the 95% confidence levels for prediction.

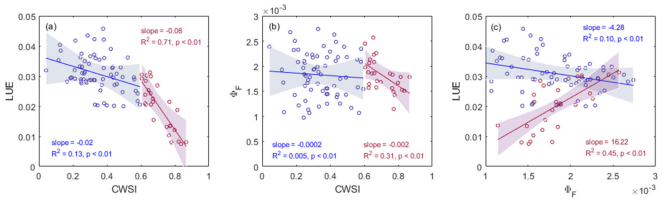

Fig. 8. Relationships between (a) LUE and (b) Φ_F and CWSI; (c) the LUE-Φ_F relationship. All the graph are for sunny days. The bule points represents data for which CWSI ≤ 0.6; the red points are for CWSI > 0.6. The shaded regions represent the 95% confidence levels for prediction.

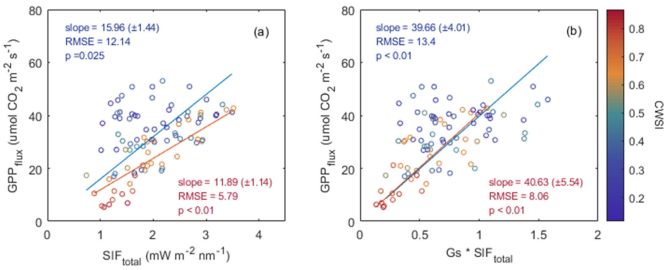

Fig. 9. Relationships between GPP and (a) $\mathrm{SIF}_{\mathrm{total}}$ and (b) Gs-SIF under drought (CWSI ≤ 0.6, blue line) and nondrought (CWSI > 0.6, red line) conditions based on measurements made on sunny days. $\mathrm{GPP}_{\mathrm{flux}}$ represents the GPP measured by EC technique. All the curves were fitted using a linear regression model with an intercept of 0. The color scale represents the CWSI value.

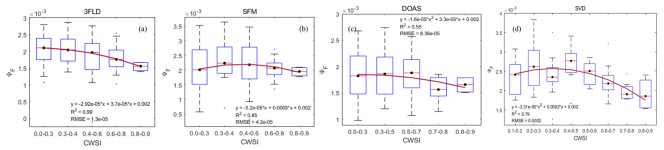

Fig. 10. Quadratic curves between Φ_F and CWSI in several intervals of CWSI based on (a) 3FLD, (b) SFM, (c) DOAS, and (d) SVD methods.

2) Seasonal Response of SIF and GPP to Drought Stress: Based on daily mean measurements, we analyzed the relationship between the ratio of GPP to SIF and the CWSI on sunny days. To avoid the influences of the early and late growth periods, we excluded the data for which the NDVI was less than 0.7. The seasonal pattern of the canopy SIF was consistent with that of the GPP over the whole growing season, and both the SIF and GPP exhibited gradual increases as the canopy developed and showed a significant decline from leaf senescence to harvest (see Figs. S7 and S8). Large number of studies have demonstrated that the PAR plays a dominant role in the close relationship between the SIF and GPP, and our observations also demonstrated this. In addition, many studies have demonstrated that the ratio of GPP to SIF exhibits a decreased trend with increasing light intensity. However, the effects of physiological factors on the SIF–GPP relationship remain unclear, especially the effects of the environmental conditions on the ratio of LUE to $\mathrm{SIF}_{\mathrm{yield}}$ (the product of Φ_F and f_{esc}). Therefore, we investigated the relationship between $\mathrm{GPP}/\mathrm{SIF}_{\mathrm{canopy}}$ (equal to $\frac{\mathrm{LUE}}{\Phi_F f_{\mathrm{esc}}}$) and the drought conditions, as characterized by the CWSI. We found that the ratio of GPP to SIF decreased when the drought stress became more severe [see Fig. 6(a)]; interestingly, the value of Gs exhibited a similar pattern in response to drought [see Fig. 6(b)]. It should be noted that the structural and physiological factors are difficult to distinguish and they both affect the close SIF–GPP relationship. In order to reduce the influence of the structural factors (as measured by f_{esc}), we compared the relationship between $\mathrm{GPP}/\mathrm{SIF}_{\mathrm{canopy}}$ and $\mathrm{GPP}/\mathrm{SIF}_{\mathrm{total}}$ as the CWSI increased. The results showed that the declined in the GPP–SIF ratio with increasing CWSI still existed (see Fig. S9) as f_{esc} changed little when NDVI ≥ 0.7.

We also found a strong dependence [$\mathrm{R}^2 = 0.89$; Fig. 7(a)] of $\frac{\mathrm{LUE}}{\Phi_F f_{\mathrm{esc}}}$ on Gs averaged over CWSI intervals of 0.2 and a higher R^2 value (0.91) for the dependence of $\frac{\mathrm{LUE}}{\Phi_F}$ on Gs. These results confirmed the hypothesis given in (19) and indicated that Gs might be a powerful indicator of the varying relationship between GPP and SIF under drought stress.

In addition, compared to two canopy structural factors (NDVI and NIRv), both the Pearson and partial correlation coefficients between Gs to the $\frac{\mathrm{LUE}}{\Phi_F}$ were higher (0.38, $p < 0.01$ and 0.32, $p < 0.01$, respectively) (see Table I; PAR was the control variable used for partial correlation). The changes in the ratio of GPP to SIF with drought stress might first be a consequence of the changes in the plant physiological status, especially the down-regulation of the carbon reaction that results from weakened stomatal reactions.

We also found that the ratio of GPP to SIF showed obvious differences between clear and cloudy weather conditions and that changes in weather conditions influenced the relationship between SIF and GPP. We, therefore, divided our measurements into "clear" and "cloudy" to analyze the differences in the response of the GPP/SIF ratio to different drought levels. The results showed that the GPP/SIF ratio was higher on cloudy days was higher than on clear days, which is a result that is consistent with previous studies [62], [68]. The GPP/SIF values decreased as the CWSI value increased under both sunny and

TABLE I
CORRELATION COEFFICIENTS FOR THE RELATIONSHIPS BETWEEN GS, NDVI, NIRV, AND THE RATIO OF GPP TO CANOPY SIF ($\mathrm{LUE}/(\Phi_F f_{\mathrm{esc}})$) AND TOTAL SIF ($\mathrm{LUE}/\Phi_F$) FOR A MAIZE FIELD. BOTH THE PEARSON AND PARTIAL CORRELATION COEFFICIENTS ARE GIVEN (CONTROL VARIABLES IN PARENTHESES)

Variables	Pearson's correlation coefficient		Partial correlation coefficient					
			(PAR)		(Ta)		(CWSI)	
	$LUE/(\Phi_F f_{esc})$	LUE/Φ_F	$LUE/(\Phi_F f_{esc})$	LUE/Φ_F	$LUE/(\Phi_F f_{esc})$	LUE/Φ_F	$LUE/(\Phi_F f_{esc})$	LUE/Φ_F
Gs	**0.39****	**0.38****	**0.35****	**0.32****	**0.29****	**0.31****	0.17	0.10
NDVI	0.04	0.23*	-0.06	0.13	-0.03	0.15	-0.19	0.03
NIRv	0.14	**0.32****	0.05	**0.28****	0.07	**0.29****	-0.10	0.17

*Represents a significance level of 0.05.
**Represents a significance level of 0.01.

cloudy conditions (see Fig. S10), but this relationship was more significant on sunny days.

It should be noted that the decreased trend of the ratio of LUE to Φ_F with increasing CWSI values attributed to both contributions of LUE and Φ_F (see Figs. 3 and 7). Under slight drought conditions, there might exist an increase Φ_F under the same LUE value because SIF is a way of energy dissipation. The same results can also be found from the SCOPE simulation data (see Fig. S5).

B. Ability of Φ_F to Track LUE Changes Under Drought Stress

Because of the effect of weather conditions had on the SIF–GPP relationships, we only analyzed the influence of CWSI on the LUE $-\Phi_F$ relationship on sunny days. Obvious difference in the LUE$-\Phi_F$ relationship was found between sunny days classed as "drought" and "nondrought" (using CWSI > 0.6 as the definition of drought). There was a smaller drop in Φ_F than in LUE when the drought became severe. This may result from the response of the light reactions being muted compared to the stomatal response, which results from an increase in NPQ and the proportion of open PSII reaction centers compensating for decreases in photochemistry, thus dampening the impact on the SIF [see Fig. 8(a) and (b)]. The large down-regulation of the LUE can be attributed to the fall in Gs [see Fig. 6(b)]. However, the lower Φ_F values might result from attenuation of the PSII activity attenuated or the complexity regulation mechanisms of the NPQ. However, a positive relationship between LUE and Φ_F was found under drought conditions [see Fig. 8(c)], which indicates that Φ_F can be a powerful parameter for tracking LUE under these conditions.

C. Comparison of SIF-Based Estimates of GPP With and Without Gs Under Drought Stress

We assessed the performance of the estimates of the GPP based on the SIF under drought stress that had been made and considered the effect of Gs parameters on these estimates. We divided the estimates made on sunny days into "drought" (CWSI > 0.6) and "nondrought" (CWSI$< = 0.6$). We used linear equations to represent the relationship between the total SIF and GPP under drought and nondrought conditions [see Fig. 9(a)]. We, then, explored the effect of the Gs parameter on the SIF-based GPP estimation model and constructed a similar linear relationship between SIF$\times$ Gs and GPP [see Fig. 9(b)]

From the results, the SIF–GPP relationship is highly significant under drought stress ($p<0.01$) and has a lower value of the root mean squared error (RMSE, 5.79) than under nondrought conditions (RMSE $= 12.14$, $p = 0.025$). This possibly indicates that Φ_F is better able to track the LUE under drought conditions and that the SIF is a better indicator of the changes in GPP under environmental stress. In addition, there is a significant difference in slopes of the SIF-based GPP estimates between drought (slope $= 15.96\pm1.44$) and nondrought (slope $= 11.89\pm1.14$). These results also confirm that drought stress significantly affects the SIF–GPP relationship. Furthermore, we found that Gs had a significant effect on the SIF-based GPP estimation models (Gs–SIF-based) under drought (RMSE $= 8.06$, $p < 0.01$) and nondrought conditions (RMSE $= 13.4$, $p < 0.01$). When Gs was considered, the slopes for drought (40.63 ± 5.54) and nondrought (39.66 ± 4.01) days were almost the same [see Fig. 9(b)], indicating that Gs can be used to correct for the effects of drought on the SIF–GPP relationship. However, it should be noted that Gs is affected by various environmental conditions and the uncertainties of the retrieval method according to the PM equation [27], [56].

The abovementioned results shows that Gs is a sensitive parameter that reflects the environmental stress experienced by plants and could be used to reduce the uncertainties in GPP estimation based on SIF. Therefore, under drought conditions, care should be taken when making estimates of the GPP based on SIF. However, it may be possible to reduce the uncertainties in these estimates by combing the use of the SIF and Gs, based on the assumption that Gs can reflect the changes in $\frac{\mathrm{LUE}}{\Phi_F}$ that result from changes in the environmental conditions ($\frac{\mathrm{GPP}}{\mathrm{SIF_{total}}} = \frac{\mathrm{LUE}}{\Phi_F}$, Fig. 7).

IV. DISCUSSION

A. Factors Constraining the SIF-GPP Relationship Under Drought Conditions

In this article, we analyzed the diurnal and seasonal SIF–GPP relationships under different stress levels, as expressed by the CWSI. The judgments of the water stress are complex and include the soil deficit and the demand for air and water, etc. The CWSI drought index has been shown to be an effective indicator for detecting crop drought [59], [69]. Our results showed that drought influenced the relationship between SIF and GPP and that the ratio of GPP to SIF decreased as the stress level increased (as validated using the field-measured and the SCOPE-simulated

data, respectively). These results are consistent with those of previous studies [7], [8], [28], [70]. The strong link between LUE and Φ_F under drought stress found using daily measurements agrees with the ideas proposed by Wieneke *et al.* [70] that the structural-eliminated Φ_F is strong dependent on the seasonal and diurnal LUE, in particular under drought stress (see Fig. 8).

The potential factors affecting the different responses of SIF and GPP to drought might be attributable to the upregulation of NPQ. The response of light reactions may be muted compared to the stomatal response as an increase in NPQ and the proportion of open PSII reaction centers compensates for decreases in photochemistry, dampening the impact on the SIF (see Fig. 3 and 8; [2], [12]). In our article, we found that, under drought stress, that there was a smaller drop in Φ_F than in the LUE and that this phenomenon might result from the complex regulation mechanism for dissipating excess energy by NPQ (see Fig. 1).

However, the different responses of the SIF and GPP to drought might also be a result of the light reactions and carbon reactions of photosynthesis operating at different time scales [12]. Because the stomatal response to drought is faster than that of the electron transport, which is directly related to the SIF, this may alter the SIF–GPP relationship. Thus, the value of SIF as an accurate estimator of photosynthesis may decrease during mild stress events of short duration, especially when the response is primarily stomatal and not fully coupled with the light reactions of photosynthesis. Souza *et al.* [17] reported that water-stressed plants exhibited reductions in CO_2 assimilation rates that were paralleled by reductions in Gs and transpiration rates. Zhang *et al.* [18] found that stomatal limitation on photosynthesis were dominant in the mooring but nonstomatal limitation was dominant in the afternoon and stomatal limitation was dominant for mild drought. Recently, Helm *et al.* [19] found a strong stomatal response to drought stress, as evidenced by decreases in net photosynthetic carbon assimilation and Gs, whereas SIF showed a weaker drought response in eastern cottonwood. Therefore, the changes in the ratio of GPP to SIF with drought stress might first result from changes in the plant physiological status, particularly the down-regulated carbon reaction resulting from weak stomatal reactions. In this article, we also found that there was a smaller drop in Φ_F than in LUE when the drought became severe. It may be that the response of the light reactions may be more muted than that of the stomatal response as a result of an increase in NPQ and the proportion of open PSII reaction centers compensating for decreases in photochemistry, thus dampening the impact on the SIF [see Fig. 3; Fig. 8(a) and (b)].

We also estimated the performance of different SIF retrieval methods on the results. Based on the results retrieved by 3FLD, SFM, DOAS, and SVD method, we could clearly observe that the nonlinear response of Φ_F to CWSI (see Fig. 10). We could conclude that Φ_F was nonlinear related to the drought conditions. However, it needs further study about the potential changeable mechanism of Φ_F with drought conditions at leaf scales.

In addition, during drought conditions, plants may experience a combination of both canopy structural changes and physiological stress. Therefore, due to the complex adaptation strategies and responses of plants under drought conditions [70], the use of SIF to estimate GPP at different spatiotemporal scales and for different plant types requires careful consideration.

B. Uncertainties in SIF-Based GPP Estimation Models

In this article, we compared SIF-based GPP estimation models that did and not include Gs. We first built a linear SIF–GPP model, which assumed that the ratio $\frac{\mathrm{LUE}}{\Phi_F}$ was constant (15). Second, we investigated the influence of the Gs parameter on the SIF-based GPP estimation model based on the hypothesis that the redox state of the chloroplast plastoquinone A ($\mathrm{Q_A}$) might be signaled to the stomatal guard cells instead of a photosynthesis-derived signal [25], [26]. The results showed that the SIF–GPP relationship was highly significant under drought stress ($p < 0.01$) and had a lower value of the root-mean-squared error (5.79) than under nondrought conditions (12.14, $p = 0.025$). It was also found that, for the SIF-based GPP estimates, there was a significant difference in slopes between drought (slope $=$ 15.96 ± 1.44) and nondrought (slope $= 11.89 \pm 1.14$) conditions. Finally, it was found that Gs has the potential for use as an indicator for describing the changes in the relationship between SIF and GPP under drought conditions and that the mechanism behind this should be further explored.

Irrespective of the uncertainties regarding the mechanism behind the strong dependence of any given photosynthetic parameter on Gs, this article demonstrates how the down-regulation of the whole photosynthetic process as drought progresses is integrated, which is in accordance with theories of integrated "photosynthetic control" [71]. This integrated regulation of photosynthesis has indicated that there has some correlation between Gs and some fluorescence parameter [24], [72]. The Gs critically determines the photosynthetic uptake of CO_2 and the amount of water transpired from leaves. Some researchers have used a "big-leaf" description of the plant canopy and estimated the GPP by assuming that the transport of CO_2 from the bulk air to the intercellular leaf space is limited by molecular diffusion through the stomata [61], [63], [64]. The GPP estimation equation can be expressed as

$$\mathrm{GPP} = \frac{G_s}{1.6}\left(1 - R_0\right) C_a + R_e \tag{20}$$

where G_s ($mol\ H_2O\ m^{-2}s^{-1}$) is the canopy conductance of water vapor; $R_0 = C_i/C_a$ and is the minimum ratio of the internal (C_i) to the external (C_a) CO_2 concentration ($mol\ mol^{-1}$), R_e is the ecosystem respiration. The constant 1.6 relates G_s to the CO_2 conductance in molar units (G_c, $mol\ CO_2\ m^{-2}s^{-1}$) (this follows from the ideal gas law for standard air pressure and a temperature of 25 °C, divided by 1.6 to account for the lesser diffusivity of CO_2 compared to H_2O). Generally, it can be assumed that R_0 is constant (0.89 under optimal conditions) for a given vegetation community—or at least is relatively narrowly constrained. Equation (20) can, then, be used to estimate the maximum rate of CO_2 uptake for a given value of G_s [66], [67]. However, we found that the relationship between GPP and Gs was not high enough with a R^2 value of 0.2 (see Fig. S12). Gs is greatly affected by drought stress, which results in a down-regulation of the whole process of photosynthesis due

to the decreased CO_2 availability [64]; the stomatal movements are very dynamic due to complex regulation by multiple factors. In our article, we also observed that Gs is sensitive to changes in environmental conditions as measured by the CWSI (see Figs. 3–6). However, it should be noted that Gs is affected by a variety of environmental factors and that there are large uncertainties in the retrieval results using the PM equation [27], [56]. In addition, prediction of Gs is a key element in the scaling-up of leaf-level gas exchange processes to canopy, ecosystem, and land surface models. Gs can be estimated from Gs models [73], [74]. In this article, we obtained Gs by inverting the PM equation using eddy-covariance data; as a result, there were large uncertainties in the value of Gs due to the complex parameter inputs to the PM equation. Furthermore, it would be worthwhile to investigate the use of Gs values calculated using the Ball-Berry model for Gs-SIF based GPP estimates as this model has been shown to provide a good description of atmosphere exchange mechanisms [19], [75].

In addition, many photosynthetic parameters (e.g., the electron transport rate, carboxylation efficiency, intrinsic water-use efficiency, respiration rate under illumination, etc.) are also more strongly correlated with the Gs than with the water content itself. Moreover, steady-state chlorophyll fluorescence has also been shown to have a high dependence on Gs [64]. Stomata close progressively as drought progresses and this is followed by a parallel decrease in net photosynthesis. However, the Gs is not controlled by the soil water availability alone, but by a complex interaction between factors internal and external to the leaf. Stomata often close in response to drought before any change in the leaf water potential and/or leaf water content is detectable [76]. It is now well established that there exists a drought-induced root-to-leaf signaling, initiated by the drying out of the soil and which reaches the leaves through the transpiration stream, which induces closure of stomata. This chemical signal has been shown to be abscisic acid (ABA), which is synthesized in the roots in response to the drying of the soil [77]. Finally, stomata also close as the leaf-to-air VPD increases irrespective of soil water availability. Stomata close progressively as drought progresses, followed by a parallel decrease in net photosynthesis. This complex regulation of Gs is related to the importance of stomata to the leaf water potential, relative water content, ABA, and other parameters, making it difficult to define a pattern of photosynthetic response to drought. Nevertheless, it must be emphasized that a high degree of coregulation between the Gs and photosynthesis is usually found [63]. Since Gs is responsive to all the external (soil water availability and VPD) and internal (ABA, xylem conductivity and leaf water status) factors related to drought, it represents a more integrated basis for considering the overall effects of drought than the leaf water potential and relative water content. Previous studies have reported that, when light-saturated Gs was used as the reference parameter to reflect drought intensity, a common response pattern was observed and this pattern was much less dependent on the particular species and conditions [64]. Therefore, in searching for a common pattern of photosynthetic response to drought, we used Gs as an integrated parameter that reflects the water stress experienced by the plant. However, the mechanism linking Gs and the coefficient ($\frac{\mathrm{LUE}}{\Phi_F}$) and the extent of the influence of different types of environmental stress require further exploration.

C. Limitations of This Article

In this article, we only explored the continuously measured maize data. Maize is a typical C4 plant and the results might be different for C3 plants. For C3 plants, studies have demonstrated that drought stress causes a decrease in net photosynthesis but has a smaller effect on the electron transport rate; it is, likely that this is because photorespiration serves as an alternative sink for electrons in these plants [12], [19], [63]. An increase in photorespiration induced by drought stress might alter the relationship between the net photosynthetic carbon exchange and the light reactions in photosynthesis [23], [78], [79]. This may be a result of the response of the photosynthetic light and carbon reactions operating on different timescales [12].

In this article, maize was taken as being representative of the C4 plant family and the plants used were routinely irrigated. Due to the different photosynthetic processes in C3 and C4 plants, LUE and $\mathrm{SIF}_{\mathrm{yield}}$ might exhibit different response mechanisms to changing environmental stresses. Compared with C3 crops, C4 crops have a higher light capacity and adaptability to high temperatures [80]. Furthermore, C3 leaves exhibit a more pronounced reduction in carbon absorption than C4 leaves around noon when the Gs decreases due to the high evaporation demand [81], [82]. Therefore, it can be inferred that the influence of drought events on the SIF–GPP relationship for C3 plants may be greater than for C4 plants. In the absence of photorespiration, maize might be more susceptible to be drought. However, due to the limited data available, the results of our study might only apply to C4 plants.

In summary, SIF varies across species and with the environmental conditions due to changes in the canopy structure, leaf chlorophyll content, leaf area index, and other plant physiological or leaf biochemical properties [83]–[85]. Therefore, the impacts of environmental conditions should be carefully considered when using SIF to estimate GPP at the global scale.

V. Conclusion

In this article, we investigated the link between the SIF and GPP at diurnal and seasonal timescales for a maize field and the response of this relationship to drought using three-year time-series of data obtained from tower-based measurements. The drought conditions were defined by the CWSI.

We found the SIF–GPP relationship was significantly affected by the drought stress and the ratio of GPP to SIF exhibited a decreasing trend as the drought became more severe. This conclusion was also confirmed by SCOPE simulation results. Interestingly, the results also showed that the ratio of GPP to SIF changed in a similar way to the canopy Gs in response to drought stress. Gs might, therefore, be a good indicator for the responses of GPP and SIF to changing environmental conditions. The changes in the ratio of GPP to SIF with drought stress might first be variations in the plants' physiological status, especially

the down regulation of the carbon reaction that resulted from weakened stomatal reactions. We also found that Φ_F tracked the changes in LUE well under drought (CWSI>0.6) conditions, which demonstrates that SIF is a powerful parameter for estimating GPP under drought stress. However, the drop in Φ_F was smaller with increasing CWSI values than LUE. The slope between Φ_F and CWSI (–0.002) was lower than that between LUE and CWSI (–0.08). It may be that the response of the light reactions was muted compared to the stomatal response as the increase in NPQ and the proportion of open PSII reaction centers compensated for decreases in photochemistry, dampening the impact on the SIF. This article, thus, contributes to a better understanding of the effects of drought on the relationship between GPP and SIF and emphasizes that Gs carries a large amount of environmental information that is important to the SIF-based models for estimating GPP. It also provides reliable evidence that the SIF carries a large amount of physiological information and can serve as a potential indicator for detecting drought and better estimating GPP.

REFERENCES

[1] D. S. Schimel, "Terrestrial ecosystems and the carbon cycle," *Global Change Biol.*, vol. 1, no. 1, pp. 77–91, 1995.

[2] G. S. Schlau-Cohen and J. Berry, "Photosynthetic fluorescence, from molecule to planet," *Phys. Today*, vol. 68, no. 9, pp. 66–67, 2015.

[3] C. Beer *et al.*, "Terrestrial gross carbon dioxide uptake: Global distribution and covariation with climate," *Science*, vol. 329, no. 5993, pp. 834–838, 2010.

[4] J. Berry *et al.*, "A coupled model of the global cycles of carbonyl sulfide and CO2: A possible new window on the carbon cycle," *J. Geophysical Res., Biogeosciences*, vol. 118, no. 2, pp. 842–852, 2013.

[5] A. Damm, L. Guanter, V. C. Laurent, M. E. Schaepman, A. Schickling, and U. Rascher, "FLD-based retrieval of sun-induced chlorophyll fluorescence from medium spectral resolution airborne spectroscopy data," *Remote Sens. Environ.*, vol. 147, pp. 256–266, 2014.

[6] Z. Ni *et al.*, "Early water stress detection using leaf-level measurements of chlorophyll fluorescence and temperature data," *Remote Sens.*, vol. 7, no. 3, pp. 3232–3249, 2015.

[7] C. Frankenberg *et al.*, "New global observations of the terrestrial carbon cycle from GOSAT: Patterns of plant fluorescence with gross primary productivity," *Geophysical Res. Lett.*, vol. 38, no. 17, pp. 236–251, 2011.

[8] L. Guanter *et al.*, "Retrieval and global assessment of terrestrial chlorophyll fluorescence from GOSAT space measurements," *Remote Sens. Environ.*, vol. 121, pp. 236–251, 2012.

[9] N. R. Baker, "Chlorophyll fluorescence: A probe of photosynthesis in vivo," *Annu. Rev. Plant Biol.*, vol. 59, pp. 89–113, 2008.

[10] E. H. Murchie and T. Lawson, "Chlorophyll fluorescence analysis: A guide to good practice and understanding some new applications," *J. Exp. Botany*, vol. 64, no. 13, pp. 3983–3998, 2013.

[11] P. Ciais *et al.*, "Carbon and other biogeochemical cycles," in *Proc. Climate Change 2013, Phys. Sci. Basis. Contribution Work. Group I to 5th Assessment Rep. Intergovernmental Panel Climate Change*, Cambridge Univ. Press, Cambridge, U.K., 2014, pp. 465–570.

[12] L. Gu, J. Han, J. D. Wood, C. Y. Y. Chang, and Y. Sun, "Sun-induced Chl fluorescence and its importance for biophysical modeling of photosynthesis based on light reactions," *New Phytologist*, vol. 223, no. 3, pp. 1179–1191, 2019.

[13] N. C. Parazoo *et al.*, "Terrestrial gross primary production inferred from satellite fluorescence and vegetation models," *Global Change Biol.*, vol. 20, no. 10, pp. 3103–3121, 2014.

[14] Y. Sun *et al.*, "Drought onset mechanisms revealed by satellite solar-induced chlorophyll fluorescence: Insights from two contrasting extreme events," *J. Geophysical Res., Biogeosciences*, vol. 120, no. 11, pp. 2427–2440, 2015.

[15] B. Osmond, M. Badger, K. Maxwell, O. Björkman, and R. Leegood, "Too many photons: Photorespiration, photoinhibition and photooxidation," *Trends Plant Sci.*, vol. 2, no. 4, pp. 119–121, 1997.

[16] U. Schreiber and C. Neubauer, "O2-dependent electron flow, membrane energization and the mechanism of non-photochemical quenching of chlorophyll fluorescence," *Photosynthesis Res.*, vol. 25, no. 3, pp. 279–293, 1990.

[17] R. Souza, E. Machado, J. Silva, A. Lagôa, and J. Silveira, "Photosynthetic gas exchange, chlorophyll fluorescence and some associated metabolic changes in cowpea (Vigna unguiculata) during water stress and recovery," *Environ. Exp. Botany*, vol. 51, no. 1, pp. 45–56, 2004.

[18] Y. Zhang *et al.*, "Effect of water stress on photosynthesis, chlorophyll fluorescence parameters and water use efficiency of common reed in the Hexi corridor," *Russian J. Plant Physiol.*, vol. 66, no. 4, pp. 556–563, 2019.

[19] L. T. Helm, H. Shi, M. T. Lerdau, and X. Yang, "Solar-induced chlorophyll fluorescence and short-term photosynthetic response to drought," *Ecological Appl.*, vol. 30, no. 5, 2020, Art. no. e02101.

[20] S. Long, S. Humphries, and P. G. Falkowski, "Photoinhibition of photosynthesis in nature," *Annu. Rev. Plant Biol.*, vol. 45, no. 1, pp. 633–662, 1994.

[21] K. Saccardy, B. Pineau, O. Roche, and G. Cornic, "Photochemical efficiency of photosystem II and xanthophyll cycle components in Zea mays leaves exposed to water stress and high light," *Photosynthesis Res.*, vol. 56, no. 1, pp. 57–66, 1998.

[22] Z. Cerovic, Y. Goulas, M. Gorbunov, J.-M. Briantais, L. Camenen, and I. Moya, "Fluorosensing of water stress in plants: Diurnal changes of the mean lifetime and yield of chlorophyll fluorescence, measured simultaneously and at distance with a τ-LIDAR and a modified PAM-fluorimeter, in maize, sugar beet, and kalanchoë," *Remote Sens. Environ.*, vol. 58, no. 3, pp. 311–321, 1996.

[23] J. Flexas *et al.*, "Steady-state chlorophyll fluorescence (Fs) measurements as a tool to follow variations of net CO2 assimilation and stomatal conductance during water-stress in C3 plants," *Physiologia Plantarum*, vol. 114, no. 2, pp. 231–240, 2002.

[24] A. Ounis, S. Evain, J. Flexas, S. Tosti, and I. Moya, "Adaptation of a PAM-fluorometer for remote sensing of chlorophyll fluorescence," *Photosynthesis Res.*, vol. 68, no. 2, pp. 113–120, 2001.

[25] F. A. Busch, "Opinion: The red-light response of stomatal movement is sensed by the redox state of the photosynthetic electron transport chain," *Photosynthesis Res.*, vol. 119, no. 1, pp. 131–140, 2014.

[26] J. Kromdijk, K. Głowacka, and S. P. Long, "Predicting light-induced stomatal movements based on the redox state of plastoquinone: Theory and validation," *Photosynthesis Res.*, vol. 141, no. 1, pp. 83–97, 2019.

[27] J. Monteith, "Solar radiation and productivity in tropical ecosystems," *J. Appl. Ecol.*, vol. 9, no. 3, pp. 747–766, 1972.

[28] L. Guanter *et al.*, "Global and time-resolved monitoring of crop photosynthesis with chlorophyll fluorescence," *Proc. Nat. Acad. Sci.*, vol. 111, no. 14, pp. E1327–E1333, 2014.

[29] G. Miao *et al.*, "Sun-induced chlorophyll fluorescence, photosynthesis, and light use efficiency of a soybean field from seasonally continuous measurements," *J. Geophysical Res., Biogeosciences*, vol. 123, no. 2, pp. 610–623, 2018.

[30] X. Liu *et al.*, "Downscaling of solar-induced chlorophyll fluorescence from canopy level to photosystem level using a random forest model," *Remote Sens. Environ.*, vol. 231, 2019, Art. no. 110772.

[31] B. Dechant *et al.*, "Canopy structure explains the relationship between photosynthesis and sun-induced chlorophyll fluorescence in crops," *Remote Sens. Environ.*, vol. 241, 2020, Art. no. 111733.

[32] H. Kimm *et al.*, "Quantifying high-temperature stress on soybean canopy photosynthesis: The unique role of sun-induced chlorophyll fluorescence," *Global Change Biol.*, vol. 27, no. 11, pp. 2403–2415, 2021.

[33] L. Liu *et al.*, "Estimating maize GPP using near-infrared radiance of vegetation," *Sci. Remote Sens.*, vol. 2, 2020, Art. no. 100009.

[34] G. Wu *et al.*, "Radiance-based NIRv as a proxy for GPP of corn and soybean," *Environ. Res. Lett.*, vol. 15, no. 3, 2020, Art. no. 034009.

[35] H. Kirnak, H. Irik, and A. Unlukara, "Potential use of crop water stress index (CWSI) in irrigation scheduling of drip-irrigated seed pumpkin plants with different irrigation levels," *Scientia Horticulturae*, vol. 256, 2019, Art. no. 108608.

[36] R. D. Jackson, "Canopy temperature and crop water stress," in *Advances in Irrigation*, vol. 1. New York, NY, USA: Elsevier, 1982, pp. 43–85.

[37] B. N. Candogan, M. Sincik, H. Buyukcangaz, C. Demirtas, A. T. Goksoy, and S. Yazgan, "Yield, quality and crop water stress index relationships for deficit-irrigated soybean [Glycine max (L.) Merr.] in sub-humid climatic conditions," *Agricultural Water Manage.*, vol. 118, pp. 113–121, 2013.

[38] X. Hu, L. Lu, X. Li, J. Wang, and M. Guo, "Land use/cover change in the middle reaches of the Heihe river basin over 2000-2011 and its implications for sustainable water resource management," *PloS One*, vol. 10, no. 6, 2015, Art. no. e0128960.

[39] X.-D. Song *et al.*, "Mapping soil organic carbon content by geographically weighted regression: A case study in the Heihe River basin, China," *Geoderma*, vol. 261, pp. 11–22, 2016.

[40] E. K. Webb, G. I. Pearman, and R. Leuning, "Correction of flux measurements for density effects due to heat and water vapour transfer," *Quart. J. Roy. Meteorological Soc.*, vol. 106, no. 447, pp. 85–100, 1980.

[41] S. M. Liu *et al.*, "A comparison of eddy-covariance and large aperture scintillometer measurements with respect to the energy balance closure problem," *Hydrol. Earth Syst. Sci.*, vol. 15, no. 4, pp. 1291–1306, 2011.

[42] S. Liu *et al.*, "The heihe integrated observatory network: A basin-scale land surface processes observatory in China," *Vadose Zone J.*, vol. 17, no. 1, pp. 1–21, 2018.

[43] M. Reichstein *et al.*, "On the separation of net ecosystem exchange into assimilation and ecosystem respiration: Review and improved algorithm," *Global Change Biol.*, vol. 11, no. 9, pp. 1424–1439, 2005.

[44] M. Reichstein, A. Moffat, T. Wutzler, and K. Sickel, "REddyProc: Data processing and plotting utilities of (half-) hourly eddy-covariance measurements," R package version 0.6–0/r9, 2014, Art. no. 755.

[45] J. Hu, L. Liu, J. Guo, S. Du, and X. Liu, "Upscaling solar-induced chlorophyll fluorescence from an instantaneous to daily scale gives an improved estimation of the gross primary productivity," *Remote Sens.*, vol. 10, no. 10, pp. 1663–1683, 2018.

[46] L. Liu, L. Guan, and X. Liu, "Directly estimating diurnal changes in GPP for C3 and C4 crops using far-red sun-induced chlorophyll fluorescence," *Agricultural Forest Meteorol.*, vol. 232, pp. 1–9, 2017.

[47] R. Myneni and D. Williams, "On the relationship between FAPAR and NDVI," *Remote Sens. Environ.*, vol. 49, no. 3, pp. 200–211, 1994.

[48] D. A. Sims *et al.*, "Midday values of gross CO2 flux and light use efficiency during satellite overpasses can be used to directly estimate eight-day mean flux," *Agricultural Forest Meteorol.*, vol. 131, pp. 1–12, 2005.

[49] M. M. Rahman, D. Lamb, and J. Stanley, "The impact of solar illumination angle when using active optical sensing of NDVI to infer fAPAR in a pasture canopy," *Agricultural Forest Meteorol.*, vol. 202, pp. 39–43, 2015.

[50] M. Meroni *et al.*, "Remote sensing of solar-induced chlorophyll fluorescence: Review of methods and applications," *Remote Sens. Environ.*, vol. 113, no. 10, pp. 2037–2051, 2009.

[51] K. Grossmann, C. Frankenberg, T. S. Magney, S. C. Hurlock, U. Seibt, and J. Stutz, "PhotoSpec: A new instrument to measure spatially distributed red and far-red solar-induced chlorophyll fluorescence," *Remote Sens. Environ.*, vol. 216, pp. 311–327, 2018.

[52] U. Platt and J. Stutz, "Differential absorption spectroscopy," in *Differential Optical Absorption Spectroscopy*. Berlin, Heidelberg, Germany: Springer, 2008, pp. 135–174.

[53] C. Y. Chang *et al.*, "Systematic assessment of retrieval methods for canopy far-red solar-induced chlorophyll fluorescence using high-frequency automated field spectroscopy," *J. Geophysical Res., Biogeosciences*, vol. 125, no. 7, 2020, Art. no. e2019JG005533.

[54] X. Liu, J. Guo, J. Hu, and L. Liu, "Atmospheric correction for tower-based solar-induced chlorophyll fluorescence observations at O2-A band," *Remote Sens.*, vol. 11, no. 3, pp. 355–371, 2019.

[55] Y. Zeng, G. Badgley, B. Dechant, Y. Ryu, M. Chen, and J. A. Berry, "A practical approach for estimating the escape ratio of near-infrared solar-induced chlorophyll fluorescence," *Remote Sens. Environ.*, vol. 232, 2019, Art. no. 111209.

[56] H. L. Penman, "Natural evaporation from open water, bare soil and grass," *Proc. Roy. Soc. London. Ser. A. Math. Phys. Sci.*, vol. 193, no. 1032, pp. 120–145, 1948.

[57] X. Li *et al.*, "A simple and objective method to partition evapotranspiration into transpiration and evaporation at eddy-covariance sites," *Agricultural Forest Meteorol.*, vol. 265, pp. 171–182, 2019.

[58] C. Lin, P. Gentine, Y. Huang, K. Guan, H. Kimm, and S. Zhou, "Diel ecosystem conductance response to vapor pressure deficit is suboptimal and independent of soil moisture," *Agricultural Forest Meteorol.*, vol. 250, pp. 24–34, 2018.

[59] S. B. Idso, "Non-water-stressed baselines: A key to measuring and interpreting plant water stress," *Agricultural Meteorol.*, vol. 27, no. 1/2, pp. 59–70, 1982.

[60] L. Testi, D. Goldhamer, F. Iniesta, and M. Salinas, "Crop water stress index is a sensitive water stress indicator in Pistachio trees," *Irrigation Sci.*, vol. 26, no. 5, pp. 395–405, 2008.

[61] M. Yebra, A. I. Van Dijk, R. Leuning, and J. P. Guerschman, "Global vegetation gross primary production estimation using satellite-derived light-use efficiency and canopy conductance," *Remote Sens. Environ.*, vol. 163, pp. 206–216, 2015.

[62] J. Chen, X. Liu, S. Du, Y. Ma, and L. Liu, "Integrating sif and clearness index to improve maize GPP estimation using continuous tower-based observations," *Sensors*, vol. 20, no. 9, pp. 2493–2501, 2020.

[63] G. D. Farquhar, S. Von Caemmerer, and J. A. Berry, "Models of photosynthesis," *Plant Physiol.*, vol. 125, no. 1, pp. 42–45, 2001.

[64] H. Medrano, J. M. Escalona, J. Bota, J. Gulías, and J. Flexas, "Regulation of photosynthesis of C3 plants in response to progressive drought: Stomatal conductance as a reference parameter," *Ann. Botany*, vol. 89, no. 7, pp. 895–905, 2002.

[65] G. D. Farquhar, S. v. von Caemmerer, and J. A. Berry, "A biochemical model of photosynthetic CO2 assimilation in leaves of C3 species," *Planta*, vol. 149, no. 1, pp. 78–90, 1980.

[66] E.-D. Schulze, F. M. Kelliher, C. Körner, J. Lloyd, and R. Leuning, "Relationships among maximum stomatal conductance, ecosystem surface conductance, carbon assimilation rate, and plant nitrogen nutrition: A global ecology scaling exercise," *Annu. Rev. Ecol. Systematics*, vol. 25, no. 1, pp. 629–662, 1994.

[67] A. Tuzet, A. Perrier, and R. Leuning, "A coupled model of stomatal conductance, photosynthesis and transpiration," *Plant, Cell Environ.*, vol. 26, no. 7, pp. 1097–1116, 2003.

[68] A. Damm *et al.*, "Remote sensing of sun-induced fluorescence to improve modeling of diurnal courses of gross primary production (GPP)," *Global Change Biol.*, vol. 16, no. 1, pp. 171–186, 2010.

[69] A. Durigon and Q. d. J. van Lier, "Canopy temperature versus soil water pressure head for the prediction of crop water stress," *Agricultural Water Manage.*, vol. 127, pp. 1–6, 2013.

[70] S. Wieneke *et al.*, "Linking photosynthesis and sun-induced fluorescence at sub-daily to seasonal scales," *Remote Sens. Environ.*, vol. 219, pp. 247–258, 2018.

[71] C. Foyer, R. Furbank, J. Harbinson, and P. Horton, "The mechanisms contributing to photosynthetic control of electron transport by carbon assimilation in leaves," *Photosynthesis Res.*, vol. 25, no. 2, pp. 83–100, 1990.

[72] J. Flexas and H. Medrano, "Drought-inhibition of photosynthesis in C3 plants: Stomatal and non-stomatal limitations revisited," *Ann. Botany*, vol. 89, no. 2, pp. 183–189, 2002.

[73] P. Jarvis, "The interpretation of the variations in leaf water potential and stomatal conductance found in canopies in the field," *Philos. Trans. Roy. Soc. London. B, Biol. Sci.*, vol. 273, no. 927, pp. 593–610, 1976.

[74] J. T. Ball, I. E. Woodrow, and J. A. Berry, "A model predicting stomatal conductance and its contribution to the control of photosynthesis under different environmental conditions," in *Progress in Photosynthesis Research*. Dordrecht, The Netherlands: Springer, 1987, pp. 221–224.

[75] J. Wu *et al.*, "The response of stomatal conductance to seasonal drought in tropical forests," *Global Change Biol.*, vol. 26, no. 2, pp. 823–839, 2020.

[76] T. Gollan, N. C. Turner, and E.-D. Schulze, "The responses of stomata and leaf gas exchange to vapour pressure deficits and soil water content," *Oecologia*, vol. 65, no. 3, pp. 356–362, 1985.

[77] W. J. Davies and J. Zhang, "Root signals and the regulation of growth and development of plants in drying soil," *Annu. Rev. Plant Biol.*, vol. 42, no. 1, pp. 55–76, 1991.

[78] J. Flexas, J. Escalona, and H. Medrano, "Water stress induces different levels of photosynthesis and electron transport rate regulation in grapevines," *Plant, Cell Environ.*, vol. 22, no. 1, pp. 39–48, 1999.

[79] J. Flexas, J.-M. Briantais, Z. Cerovic, H. Medrano, and I. Moya, "Steady-state and maximum chlorophyll fluorescence responses to water stress in grapevine leaves: A new remote sensing system," *Remote Sens. Environ.*, vol. 73, no. 3, pp. 283–297, 2000.

[80] J. Ehleringer and R. W. Pearcy, "Variation in quantum yield for CO2 uptake among C3 and C4 plants," *Plant Physiol.*, vol. 73, no. 3, pp. 555–559, 1983.

[81] H. Yang, X. Zhang, and G. Wang, "Relationships between stomatal character, photosynthetic character and seed chemical composition in grass pea at different water availabilities," *J. Agricultural Sci.*, vol. 142, pp. 675–681, 2004.

[82] B. S. Ripley, M. E. Gilbert, D. G. Ibrahim, and C. P. Osborne, "Drought constraints on C4 photosynthesis: Stomatal and metabolic limitations in C3 and C4 subspecies of alloteropsis semialata," *J. Exp. Botany*, vol. 58, no. 6, pp. 1351–1363, 2007.

[83] L. Guanter *et al.*, "Using field spectroscopy to assess the potential of statistical approaches for the retrieval of sun-induced chlorophyll fluorescence from ground and space," *Remote Sens. Environ.*, vol. 133, pp. 52–61, 2013.

[84] J. Joiner *et al.*, "Global monitoring of terrestrial chlorophyll fluorescence from moderate-spectral-resolution near-infrared satellite measurements: Methodology, simulations, and application to GOME-2," *Atmospheric Meas. Techn.*, vol. 6, no. 10, pp. 2803–2823, 2013.

[85] T. S. Magney *et al.*, "Mechanistic evidence for tracking the seasonality of photosynthesis with solar-induced fluorescence," *Proc. Nat. Acad. Sci.*, vol. 116, no. 24, pp. 11640–11645, 2019.

Jidai Chen received the master's degree in ecology from Beijing Forestry University, Beijing, China, in 2019. He is currently working toward the Doctorate degree in cartography and geographic information system with the Aerospace Information Research Institute, Chinese Academy of Sciences, Beijing, China.

His research interests include the application of solar-induced chlorophyll fluorescence, gross primary production, the global economy, and the environmental changes.

Xinjie Liu received the Ph.D. degree in cartography and geographic information system from the Institute of Remote Sensing and Digital Earth, Chinese Academy of Sciences, Beijing, China, in 2016.

He is currently an Associate Professor with Aerospace Information Research Institute, Chinese Academy of Sciences, Beijing, China. He majors in remote sensing of solar-induced chlorophyll fluorescence.

Shanshan Du received the Ph.D. degree in cartography and geographic information system from Aerospace Information Research Institute, Chinese Academy of Sciences, Beijing, China, in 2020.

She is a Postdoc with Aerospace Information Research Institute, Chinese Academy of Sciences, Beijing, China. Her research interests include retrieval and application of solarinduced chlorophyll fluorescence based on satellite observations.

Yan Ma is currently working toward the Doctorate degree in cartography and geographic information system with the Aerospace Information Research Institute, Chinese Academy of Sciences, Beijing, China.

Her research interests include the time and space expansion of the chlorophyll fluorescence satellite products.

Liangyun Liu received the Ph.D. degree in optical engineering from the Xi'an Institute of Optical and Precision Mechanics, Chinese Academy of Sciences, Xi'an, China, in 2000.

He is currently a Professor with Aerospace Information Research Institute, Chinese Academy of Sciences, Beijing, China. His research interest includes quantitative remote sensing of vegetation.